

# Quasi-linearized Polynomial Collocation Method for Solving MHD Casson Nanofluid Mixed Convection

Faraidun K. Hamasalh<sup>1,\*</sup>, Balen D. Yassin<sup>2</sup>, Shko A. Tahir<sup>3</sup>

<sup>1</sup>University of Sulaimani Polytechnic, Bakrajo Technical Institute, Sulaimani, Iraq.

<sup>2</sup>University of Sulaimani, Department of Mathematics, College of Education, Sulaimani, Iraq.

<sup>3</sup>University of Sulaimani, Department of Mathematics, College of Science, Sulaimani, Iraq.

---

## ARTICLE INFO

Received 28 March 2025  
Revised 2 June 2025  
Accepted 12 June 2025  
Published 30 June 2025

## ABSTRACT

The present study focuses on the numerical and graphical analysis of the mechanism of thermal diffusion and diffusion thermo over a mixed convection Casson fluid flow over a vertical cone with porous material under the effects of Brownian motion and thermophoresis. Using transformable variables, the proposed model is transformed into a system of non-linear ODEs. Then, the approximate solutions are established using polynomial models in conjunction with spectral collocation. The impact of some important parameters, such as the Brownian motion parameter, the Prandtl number, the magnetic parameter, the Casson parameter, the Lewis number, the Dufour parameter, the Soret number, the velocity profile, the temperature, the diffusion, the skin friction coefficient, the Nusselt number, and the Sherwood number, is examined numerically. Also, several cases are resolved and graphically compared, illustrating the improved precision of the current approach.

---

### Keywords:

Fluid Dynamics, Polynomial Interpolation, Nanofluid, Spectral Collocation.

**Citation:** F. K. Hamasalh et al.,  
J.Basrah Res. (Sci.) 51(1),182  
(2025).  
DOI:<https://doi.org/10.56714/bjrs.51.1.16>

## 1. Introduction

Non-Newtonian flows are interesting phenomena that have become highly important because of their use in engineering and applied science. A subclass of non-Newtonian fluids known as viscoelastic fluids demonstrates both a viscous and a memory effect following the removal of pressure. Blood, paints, bitumen, egg white, flour dough, and polymers are a few examples of typical viscoelastic fluids. Viscoelastic impacts are particularly important in situations where the strain rate changes suddenly, such as during contractions or expansions, pulsating flows, or during flow launch or interruption. The authors [1, 2, 19] have examined how MHD Darcy-Forchheimer Casson nanofluid flow is affected by Hall current, diffusion thermometry, and activation energy when Brownian motion and thermophoresis are present. Numerical investigation of Casson nanofluid flow with thermal radiation, Hall current, and activation energy has been reported in [10] magnetohydrodynamics. Diff Chemical Reaction and Fusion Thermo Effects on Magnetohydrodynamic Jeffrey Nanofluid over an inclined vertical plate with radiation absorption and a constant heat source has been examined by [3]. The study of electrically conducting liquids, such as electrolytes, salty water, plasma, and liquid metals,

\*Corresponding author email: faraidun.hamasalh@spu.edu.iq



©2022 College of Education for Pure Science, University of Basrah. This is an Open Access Article Under the CC by License the [CC BY 4.0](#) license.

ISSN: 1817-2695 (Print); 2411-524X (Online)  
Online at: <https://jou.jobrs.edu.iq>

is known as magnetohydrodynamics. Several engineering and industrial uses for this type of fluid exist, including power generation, magnetic drug targeting, reactor cooling, crystal growth, and MHD sensors. The strength of magnetic induction determines MHD. Because of the buoyancy forces created by changes in temperature and concentration, different transport processes can be found in nature and invention where heat and mass transfer occur in different ways. The relationships between motions and driving potentials are extremely unforeseeable at the instantaneous point of mass and heat exchange in a moving liquid. The temperature and concentration gradients produce energy fluxes. The energy circulation is caused by a gradient in composition known as the Dufour effect, whereas the mass circulation is caused by a temperature gradient known as the Soret effect. When there are variations in density within the stream regime, these results are crucial. The authors have investigated MHD Casson fluid flow characteristics ahead of a vertical porous plate that is inclined [4, 7, 14]. Unsteady natural convection over a moving vertical plate embedded in a saturated porous medium with chemical reactions, Soret, and Dufour effects has been used to express heat and mass transfer [8, 12, 13, 15]. This work primarily aims to explore the impact of diffusion thermodynamics and thermal diffusion on the MHD mixed convection flow of Casson nanofluid through a vertical cone in a porous material. A system of PDEs and related boundary conditions can be reduced to a system of ODEs using similarity transformations. The ordinary differential equations for momentum, energy, and concentration are obtained using this transformation. Polynomial spline and spectral collocation techniques are used to solve the proposed system. With the aid of graphical representation, the impact of various flow parameters on temperature, concentration, and velocity profiles is examined and evaluated. This work investigates the two-dimensional electrically conducting, incompressible, viscous, boundary-layer fluid flow containing nanofluid particles and Casson fluid.

## 2. Formulation of the problem

This work investigates the 2D, incompressible, viscous, boundary layer flow electrically conducting, containing nanofluid particles and Casson fluid approaching a vertical cone under the effect of porous media and a magnetic field with the influence of Dufour and Soret number [4, 6].

The system possesses the following properties:

1.  $C_\infty$  and  $T_\infty$  are the nanoparticle volume fraction and temperature of the surrounding fluids.
2. The  $x$ -axis represent the path of the fluid flow direction over the conic surface.
3. An external magnetic field of strength  $B_0$  is applied to the  $y$ -axis.
4.  $T_\omega$  is the expected outcome of the convective heating process, that is defined by temperature  $T_f$  and a heat transfer coefficient  $h_f$ . The nanoparticle volume fraction at the cone's surface ( $y = 0$ ) is  $C_\omega$ .
5. The equation  $\tau_1 = \tau_0 + \mu_1 \alpha^* T$  describes the rheology for a non-Newtonian fluid is

$$u_x + v_y = 0, \quad (1)$$

$$uu_x + vu_y = \left(1 + \frac{1}{\beta}\right) vu_{yy} - g\alpha_1(T, C)\cos\xi - \left(\frac{\sigma\beta_0^2}{\rho_f}\right) u - \left(\frac{\mu}{k^*}\right) u, \quad (2)$$

$$uT_x + vT_y = \alpha T_{yy} - \tau\alpha_2(T, C) - \frac{\partial q_r}{\rho C_p} + \frac{D_m k_T}{c_s c_\rho} C_{yy}, \quad (3)$$

$$uC_x + vC_y = \frac{D_m k_T}{T_m} T_{yy} + D_B C_{yy} + \frac{D_T}{T_\infty} T_{yy} - K_r(C - C_\infty), \quad (4)$$

along with the boundary conditions [3].

$$v = 0, u = 0, kT_y = h_f(T - T_f), C = C_w \quad \text{at} \quad y = 0$$

$$T \rightarrow T_\infty, C \rightarrow C_\infty \text{ and } u \rightarrow 0 \quad \text{as} \quad y \rightarrow \infty \quad (5)$$

where  $\alpha_1(T, C) = (1 - C_\infty)_{pf_\infty} \beta(T - T_\infty) + (\rho_{f_\infty} - \rho_p)(C - C_\infty)$  and  $\alpha_2(T, C) = D_B \frac{\partial C}{\partial y} \frac{\partial T}{\partial y} + \frac{D_T}{T_\infty} \left( \frac{\partial T}{\partial y} \right)^2$ . In order to solve equations (2) through (4), we present the following similarity variables:

$$\eta = \left( \frac{y}{x} \right) Ra_x^{\frac{1}{4}}, \psi = \alpha Ra_x^{\frac{1}{4}} f(\eta), \theta = \frac{T - T_\infty}{T_w - T_\infty}, \phi = \frac{C - C_\infty}{C_w - C_\infty} \quad (6)$$

Equation (6) is substituted into Equations (2), (3), and (4). With the suggested governing ODE system, one can get

$$\left( 1 + \frac{1}{\beta} \right) f^{(3)} - f'^2 + ff'' + \theta - N_r \phi - (M + K)f' = 0 \quad (7)$$

$$(1 + R_d)\theta'' + P_r f\theta' + P_r N_b \left( \theta' \phi' + \frac{N_t}{N_b} \theta'^2 \right) + P_r D_u \phi' = 0 \quad (8)$$

$$\phi'' + P_r L_e (f\phi' - K_r \phi) + \left( S_r L_e + \frac{N_t}{N_b} \right) \theta'' = 0 \quad (9)$$

The boundary conditions in (5) become

$$\begin{aligned} f(0) &= 0, f'(0) = \emptyset(0) = 1, \theta'(0) + B_i \theta(0) = -B_i \\ f' &\rightarrow 0, \theta \rightarrow 0 \text{ and } \phi \rightarrow 0 \quad \text{as } \eta \rightarrow \infty \end{aligned} \quad (10)$$

Where the velocity profile  $f$ , dimensionless temperature  $\theta$  and nanoparticle concentration  $\phi$ , are the transformable unknown variables. Additionally,  $N_r$ , Magnetic parameter  $M, K$ , Radiation parameter  $R_d$ , Prandtl number  $P_r$ , Brownian motion parameter  $N_b$ . Thermophoresis parameter  $N_t$ , Dufor parameter  $D_u$ , Lewis number  $L_e$ ,  $K_r$ ,  $S_r$ ,  $B_i$  are the physical parameters.

### 3. Solution Methodology

The non-linear of non-dimensional transformed Eqs. (7)–(9), along with conditions (10), with the use of the spline polynomial and spectral collocation method. For insurance and accuracy of the proposed work, we tackled the problem with the aid of MATLAB. To solve the problem numerically, the domain  $[0, 5]$  is considered in place of  $[0, \infty)$  since there is no significant change for  $5 < \eta$ , where  $h = 0.5$ . Let.

$$\lambda_f(x, f, f', f'', f^{(3)}, \theta, \phi) = \left( 1 + \frac{1}{\beta} \right) f^{(3)} - f'^2 + ff'' + \theta - N_r \phi - (M + K)f' \quad (11)$$

$$\lambda_\theta(x, f, \theta', \theta'', \phi) = (1 + R_d)\theta'' + P_r f\theta' + P_r N_b \left( \theta' \phi' + \frac{N_t}{N_b} \theta'^2 \right) + P_r D_u \phi' \quad (12)$$

$$\lambda_\phi(x, f, \theta'', \phi, \phi', \phi'') = \phi'' + P_r L_e (f\phi' - K_r \phi) + \left( S_r L_e + \frac{N_t}{N_b} \right) \theta'' \quad (13)$$

Applying the quasi-linearization method, we expand the Eqs. (11–13).

$$\begin{aligned} \lambda_f \left( x, f_{l+1}, f'_{l+1}, f''_{l+1}, f^{(3)}_{l+1}, \theta_{l+1}, \phi_{l+1} \right) &= \lambda_f \left( x, f_l, f'_l, f''_l, f^{(3)}_l, \theta_l, \phi_l \right) + \left[ \frac{\partial \lambda_f}{\partial f} \right]_l (f_{l+1} - f_l) \\ &+ \left[ \frac{\partial \lambda_f}{\partial f'} \right]_l (f'_{l+1} - f'_l) + \left[ \frac{\partial \lambda_f}{\partial f''} \right]_l (f''_{l+1} - f''_l) + \left[ \frac{\partial \lambda_f}{\partial f^{(3)}} \right]_l (f^{(3)}_{l+1} - f^{(3)}_l) + \left[ \frac{\partial \lambda_f}{\partial \theta} \right]_l (\theta_{l+1} - \theta_l) \\ &+ \left[ \frac{\partial \lambda_f}{\partial \phi} \right]_l (\phi_{l+1} - \phi_l) \end{aligned} \quad (14)$$

$$\begin{aligned} \lambda_\theta(x, f_{l+1}, \theta'_{l+1}, \theta''_{l+1}, \phi'_{l+1}) &= \lambda_\theta(x, f_l, \theta'_l, \theta''_l, \phi_l) + \left[ \frac{\partial \lambda_\theta}{\partial f} \right]_l (f_{l+1} - f_l) + \left[ \frac{\partial \lambda_\theta}{\partial \theta'} \right]_l (\theta'_{l+1} - \theta'_l) \\ &\quad + \left[ \frac{\partial \lambda_\theta}{\partial \phi'} \right]_l (\phi'_{l+1} - \phi'_l) \end{aligned} \quad (15)$$

$$\begin{aligned} \lambda_\phi(x, f_{l+1}, \theta''_{l+1}, \phi'_{l+1}, \phi'_{l+1}, \phi''_{l+1}) &= \lambda_\phi(x, f_l, \theta''_l, \phi_l, \phi'_l, \phi''_l) + \left[ \frac{\partial \lambda_\phi}{\partial f} \right]_l (f_{l+1} - f_l) + (\theta_{l+1} - \theta_l) \\ &\quad + \left[ \frac{\partial \lambda_\phi}{\partial \phi} \right]_l (\phi_{l+1} - \phi_l) + \left[ \frac{\partial \lambda_\phi}{\partial \phi'} \right]_l (\phi'_{l+1} - \phi'_l) + \left[ \frac{\partial \lambda_\phi}{\partial \phi''} \right]_l (\phi''_{l+1} - \phi''_l) \end{aligned} \quad (16)$$

Rearranging the Eqs (14) -(16) yields the iterative system.

$$f_l'' f_{l+1} - (2f_l' + M + K) f_{l+1}' + f_l f_{l+1}'' + \left(1 + \frac{1}{\beta}\right) f_{l+1}^{(3)} + \theta_{l+1} - N_r \phi_{l+1} = f_l f_l'' - \quad (17)$$

$$\begin{aligned} P_r \theta_l' f_{l+1} + \left[ P_r f_l + \phi_l P_r N_b + \frac{2\theta_l' N_t}{N_b} \right] \theta_{l+1}' + (1 + R_d) \theta_{l+1}'' + [P_r D_u + \theta_l' P_r N_b] \phi_{l+1}' \\ = (P_r f_l + \phi_l' P_r N_b) \theta_l + \left( \frac{2\theta_l' N_t}{N_b} - P_r N_t \right) \theta_l'^2 \end{aligned} \quad (18)$$

$$P_r L_e \phi_l' f_{l+1} + \left( S_r L_e + \frac{N_t}{N_b} \right) \theta_{l+1}'' + P_r L_e K_r \phi_{l+1} + P_r L_s f_l \phi_{l+1}' + \phi_{l+1}'' = P_r L_e f_l \phi_l' \quad (19)$$

Here the approximate solutions are given as.

$$[f(\eta)]_{l+1} = \sum_{k=0}^{N+4} a_k \eta^k, [\theta(\eta)]_{l+1} = \sum_{k=0}^{N+3} b_k \eta^k, [\phi(\eta)]_{l+1} = \sum_{k=0}^{N+3} c_k \eta^k \quad (20)$$

Where  $a_k, b_k, c_k$  are to be determined, Substituting the mentioned models (20) in equations (17)-(19), we get a linear system of equations with a dimension of  $(3N + 10) \times (3N + 10)$ . For  $l = 0$  we have.

$$f_0(\eta) = -\frac{1}{10} \eta^2 + \eta, \theta_0(\eta) = -\frac{Bi}{1+5Bi} \eta + \frac{5Bi}{1+5Bi}, \phi_0(\eta) = -\frac{1}{5} \eta + 1.$$

#### 4. Numerical results and discussions

From the figures (5), (6), and (7), we can observe that the relationship between the velocity profile  $f'(\eta)$ , temperature  $\theta(\eta)$ , nanoparticle concentration  $\phi(\eta)$ , and the Prandtl number is an inverse variation. It's shown in figure (3), (4) that by increasing the values of the Brownian motion parameter  $N_b$  we see an increase in the temperature  $\theta(\eta)$  but a decrease in the nanoparticle concentration  $\phi(\eta)$ . The effect of the magnetic parameter  $M$  can be investigated through figures (1) and (2). As shown,  $M$  the magnetic parameter varies directly with the temperature  $\theta(\eta)$  but varies inversely with the velocity profile  $f'(\eta)$ . Figures (8) and (11) illustrate that the velocity profile  $f'(\eta)$  increases when the values of the radiation parameter  $R_d$  increase but decreases when the values of the Casson parameter  $\beta$  increase. Figure (12) shows that a significant increase is observed in the temperature  $\theta(\eta)$  when the values of  $Bi$  increase. Figure (9) shows that when the values of the Lewis number  $L_e$  are raised, the concentration of nanoparticles  $\phi(\eta)$  decreases. Finally, increasing the soret number  $S_r$  improves the nanoparticle concentration  $\phi(\eta)$ , as discovered in Figure (10).

**Table 1:** Convergence speed of  $f, \theta, \phi$ .

| Iteration | $\max f_{l+1} - f_l $ | $\min a_{k,l+1} - a_{k,l} $ | $\max a_{k,l+1} - a_{k,l} $ |
|-----------|-----------------------|-----------------------------|-----------------------------|
| 1         | 5.45139e-1            | 0                           | 6.22438e-1                  |
| 2         | 8.85452e-2            | 0                           | 2.78847e-2                  |

|                  |  |  |  |
|------------------|--|--|--|
| 3                | 2.92781e-3                                       | 0  | 3.31788e-4                                   |
| 4                | 2.89428e-6                                       | 0  | 1.39862e-7                                   |
| 5                | 1.99061e-12                                      | 0  | 1.39555e-13                                  |
| <b>Iteration</b> | <b>max <math>\theta_{l+1} - \theta_l </math></b> | <b>min <math>b_{k,l+1} - b_{k,l} </math></b> | <b>max <math>b_{k,l+1} - b_{k,l} </math></b> |
| 1                | 7.08815e-2                                       | 1.26242e-9                                   | 4.90095e-2                                   |
| 2                | 2.13204e-3                                       | 7.81555e-10                                  | 1.56315e-3                                   |
| 3                | 2.18406e-4                                       | 1.01618e-10                                  | 1.08896e-4                                   |
| 4                | 1.74944e-7                                       | 8.68072e-14                                  | 7.46262e-8                                   |
| 5                | 7.54045e-14                                      | 2.69853e-19                                  | 3.01980e-14                                  |
| <b>Iteration</b> | <b>max <math>\phi_{l+1} - \phi_l </math></b>     | <b>min <math>c_{k,l+1} - c_{k,l} </math></b> | <b>max <math>c_{k,l+1} - c_{k,l} </math></b> |
| 1                | 1.27079e-1                                       | 5.16369e-9                                   | 1.42523e-1                                   |
| 2                | 5.83429e-3                                       | 0  | 1.48354e-3                                   |
| 3                | 1.34454e-4                                       | 0  | 7.38707e-5                                   |
| 4                | 8.25437e-8                                       | 0  | 2.85797e-8                                   |
| 5                | 2.58906e-14                                      | 0  | 2.68760e-14                                  |

Table 1 compares the absolute error convergence speed and the approaching unknowns  $a_k$ ,  $b_k$  and  $c_k$ s between the previous iteration  $l$  and the present iteration  $l + 1$  of the proposed models shown in Eq. (20). The efficacy and validity of our suggested approach are demonstrated by the exponential decline in the first column's absolute error.

**Table 2:** Residual error analysis of  $\lambda_f$ ,  $\lambda_\theta$ ,  $\lambda_\phi$ .

| <b>Iteration</b> | <b><math>L_\infty \lambda_f </math></b>      | <b>Min  <math>\lambda_f </math></b>      | <b>Max  <math>\lambda_f </math></b>      | <b><math>L_2 \lambda_f </math></b>      |
|------------------|--|--|--|---|
| 1                | 2.80006e-01                                  | 7.48248e-04                              | 2.06482e-01                              | 7.76626e-02                             |
| 2                | 1.80224e-02                                  | 3.36444e-04                              | 7.98663e-03                              | 5.47002e-05                             |
| 3                | 3.17647e-03                                  | 9.61209e-09                              | 2.01176e-04                              | 5.70879e-04                             |
| 4                | 3.17630e-03                                  | 8.33992e-14                              | 1.99413e-04                              | 5.78624e-04                             |
| 5                | 3.17630e-03                                  | 1.63250e-17                              | 1.99413e-04                              | 5.78624e-04                             |
| <b>Iteration</b> | <b><math>L_\infty \lambda_\theta </math></b> | <b>Min  <math>\lambda_\theta </math></b> | <b>Max  <math>\lambda_\theta </math></b> | <b><math>L_2 \lambda_\theta </math></b> |
| 1                | 1.06636e-02                                  | 7.14684e-05                              | 3.55982e-03                              | 3.37062e-3                              |
| 2                | 9.78449e-05                                  | 7.59294e-07                              | 4.07614e-05                              | 3.71828e-05                             |
| 3                | 3.45538e-05                                  | 4.48516e-10                              | 1.51233e-06                              | 5.46053e-06                             |
| 4                | 3.45540e-05                                  | 1.19391e-15                              | 1.49247e-06                              | 5.48639e-06                             |
| 5                | 3.45540e-05                                  | 1.97816e-19                              | 1.49247e-06                              | 5.48639e-06                             |
| <b>Iteration</b> | <b><math>L_\infty \lambda_\phi </math></b>   | <b>Min  <math>\lambda_\phi </math></b>   | <b>Max  <math>\lambda_\phi </math></b>   | <b><math>L_2 \lambda_\phi </math></b>   |
| 1                | 1.64966e-02                                  | 3.37775e-05                              | 7.66777e-03                              | 6.07728e-03                             |
| 2                | 5.82529e-04                                  | 4.78236e-07                              | 1.24885e-04                              | 1.53744e-04                             |
| 3                | 6.74082e-05                                  | 1.65011e-09                              | 3.25291e-06                              | 1.11284e-05                             |

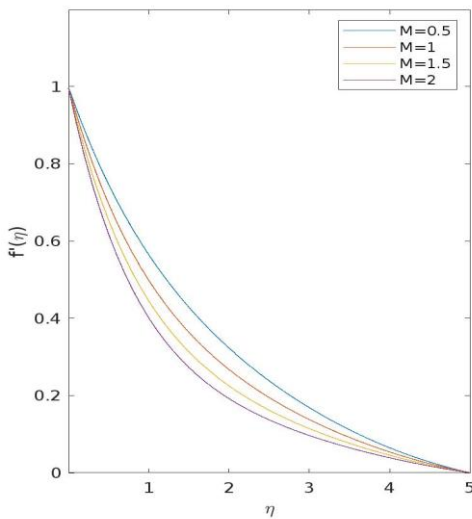
|   |             |             |             |             |
|---|-------------|-------------|-------------|-------------|
| 4 | 6.67844e-05 | 1.61438e-15 | 3.18344e-06 | 1.10163e-05 |
| 5 | 6.67844e-05 | 3.52943e-19 | 3.18344e-06 | 1.10163e-05 |

In Table 2 using the approximated spline models in (20), statistically examine the errors that are generated in Eqs. (11)–(13). Additionally, for  $\lambda_f$ ,  $\lambda_\theta$ , and  $\lambda\phi$ , the second and infinity norms are computed.

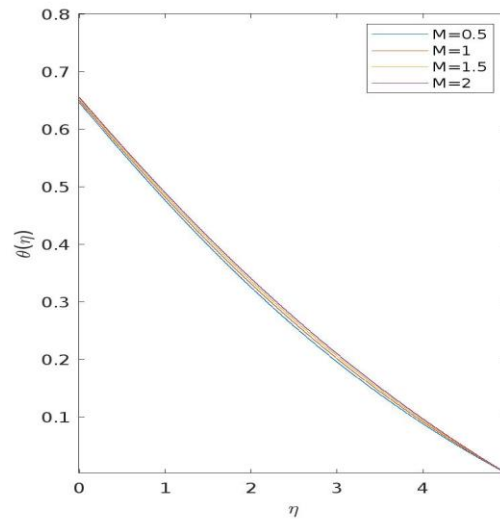
**Table 3:** Variation of non-dimensional form of the skin friction coefficient  $-2f''(0)$ , nusselt number  $-\theta'(0)$  and Sherwood number  $-\phi'(0)$ .

| $M$ | $Rd$ | $Kr$ | $Bi$ | $Nt$ | $Nb$ | $Pr$ | $Du$ | $Sr$ | $Le$ | $Re_x^{\frac{1}{2}} Cf$ | $Re_x^{\frac{1}{2}} Nu_x$ | $Re_x^{\frac{1}{2}} Sh_x$ |
|-----|------|------|------|------|------|------|------|------|------|-------------------------|---------------------------|---------------------------|
| 1.0 | 2.0  | 1.0  | 0.5  | 1.0  | 1.2  | 0.8  | 0.2  | 0.5  | 0.2  | 1.0183                  | 0.2014                    | 0.3474                    |
| 0.6 |      |      |      |      |      |      |      |      |      | 0.8901                  | 0.2029                    | 0.3486                    |
| 0.4 |      |      |      |      |      |      |      |      |      | 0.7846                  | 0.2043                    | 0.3497                    |
| 1.5 |      |      |      |      |      |      |      |      |      | 0.8984                  | 0.2031                    | 0.3487                    |
| 1.0 |      |      |      |      |      |      |      |      |      | 0.7650                  | 0.2052                    | 0.3503                    |
| 0.5 |      |      |      |      |      |      |      |      |      | 0.6140                  | 0.2077                    | 0.3523                    |
| 0.6 |      |      |      |      |      |      |      |      |      | 1.0243                  | 0.2090                    | 0.3337                    |
| 0.3 |      |      |      |      |      |      |      |      |      | 1.0310                  | 0.2173                    | 0.3188                    |
| 0.1 |      |      |      |      |      |      |      |      |      | 1.0411                  | 0.2295                    | 0.2967                    |
| 1.2 |      |      |      |      |      |      |      |      |      | 1.0135                  | 0.2035                    | 0.4983                    |
| 1.4 |      |      |      |      |      |      |      |      |      | 1.0125                  | 0.2039                    | 0.5350                    |
| 1.6 |      |      |      |      |      |      |      |      |      | 1.0115                  | 0.2043                    | 0.5699                    |
| 0.5 |      |      |      |      |      |      |      |      |      | 1.0667                  | 0.1713                    | 0.3476                    |
| 1.5 |      |      |      |      |      |      |      |      |      | 0.9982                  | 0.2140                    | 0.3474                    |
| 2.0 |      |      |      |      |      |      |      |      |      | 0.9872                  | 0.2208                    | 0.3474                    |
| 1.0 |      |      |      |      |      |      |      |      |      | 1.0188                  | 0.2028                    | 0.3542                    |
| 0.8 |      |      |      |      |      |      |      |      |      | 1.0192                  | 0.2043                    | 0.3617                    |
| 0.5 |      |      |      |      |      |      |      |      |      | 1.0198                  | 0.2064                    | 0.3744                    |
| 0.6 |      |      |      |      |      |      |      |      |      | 1.0201                  | 0.2026                    | 0.3268                    |
| 0.3 |      |      |      |      |      |      |      |      |      | 1.0245                  | 0.2025                    | 0.2529                    |
| 0.1 |      |      |      |      |      |      |      |      |      | 1.0329                  | 0.1937                    | 0.0707                    |
| 0.8 |      |      |      |      |      |      |      |      |      | 1.0661                  | 0.2913                    | 0.6589                    |
| 1.4 |      |      |      |      |      |      |      |      |      | 1.0979                  | 0.3514                    | 0.9044                    |
| 2.0 |      |      |      |      |      |      |      |      |      | 1.1172                  | 0.3888                    | 1.1269                    |
| 0.4 |      |      |      |      |      |      |      |      |      | 1.0151                  | 0.1969                    | 0.3558                    |
| 0.2 |      |      |      |      |      |      |      |      |      | 1.0087                  | 0.1877                    | 0.3729                    |
| 0.5 |      |      |      |      |      |      |      |      |      | 1.0187                  | 0.2012                    | 0.3372                    |
| 1.0 |      |      |      |      |      |      |      |      |      | 1.0194                  | 0.2007                    | 0.3205                    |
| 1.1 |      |      |      |      |      |      |      |      |      | 1.0177                  | 0.2018                    | 0.3651                    |
| 1.2 |      |      |      |      |      |      |      |      |      | 1.0170                  | 0.2021                    | 0.3824                    |

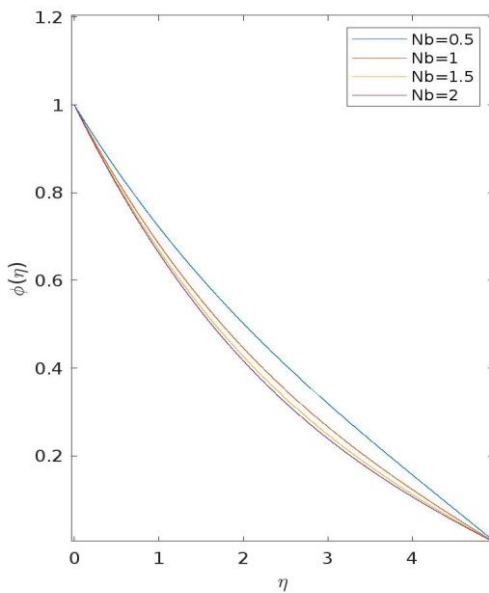
According to Table 3, skin friction increases as the Casson parameter  $\beta$ , magnetic parameter M, and Prandtl number Pr increase, while the skin friction coefficient decreases as the values of the Brownian motion parameters  $N_b$ ,  $K_r$  increase. The Nusselt number also rises with improvements in the Dufour parameter  $D_u$ , the Prandtl number  $P_r$ , the Brownian motion parameter  $N_b$ , and the  $B_i$ . In contrast, the Sherwood number varies inversely when the values of the Soret number  $S_r$ , the Dufour parameter  $D_u$ ,  $B_i$ , and the magnetic parameter M increase. The Sherwood number rises when the values of the Lewis number  $L_e$ , the Pradtl number  $P_r$ , the Brownian motion parameter  $N_b$ ,  $K_r$ , and the Radiation parameter  $R_d$  are raised.



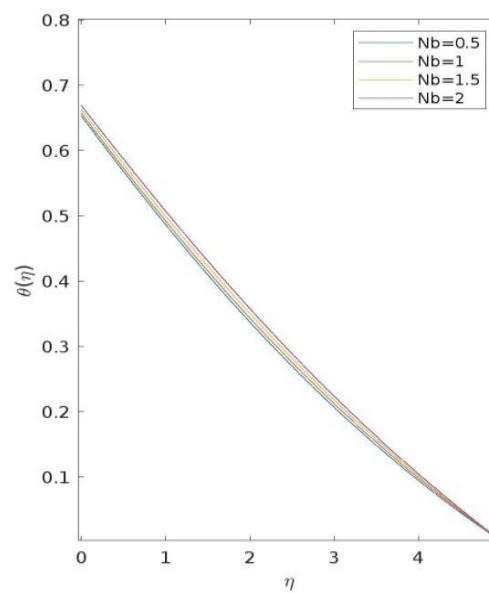
**Fig.1.** Variation of  $f'$  under influence of M.



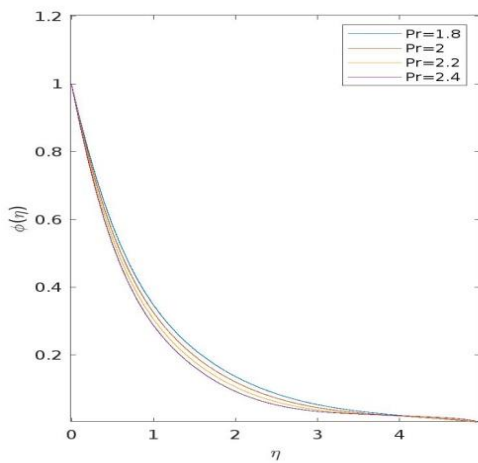
**Fig.2.** Variation of  $\theta$  under effect of M.



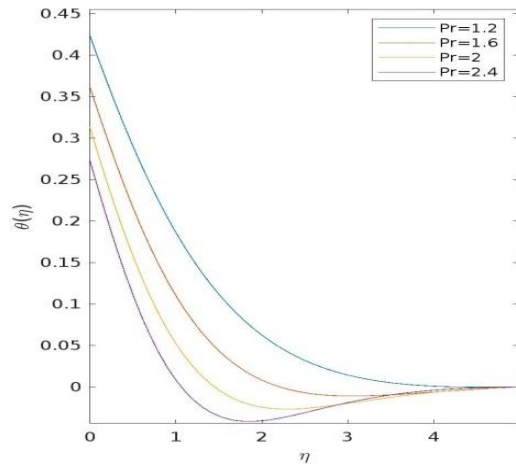
**Fig.3.** Influence of Nb on  $\phi$ .



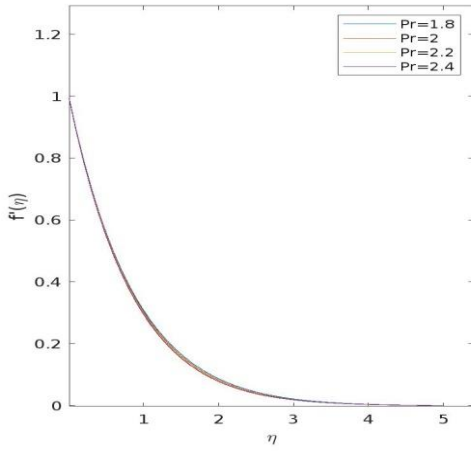
**Fig.4.** Impact of Nb over  $\theta$ .



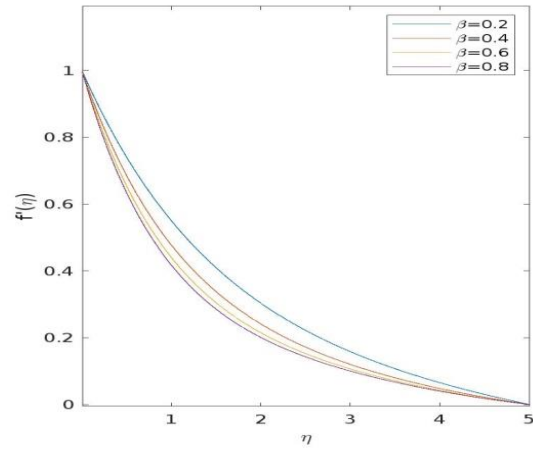
**Fig.5.** Effect of Pr on  $\phi$ .



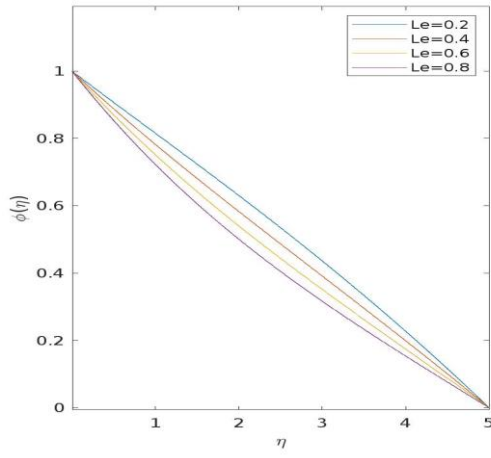
**Fig.6.** Impact of Pr over  $\theta$ .



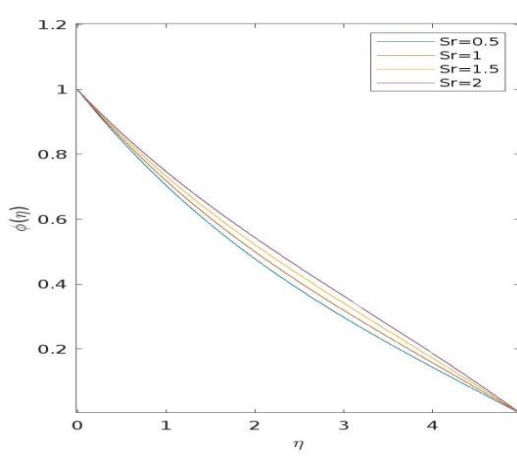
**Fig.7.** Variation of  $f'$  under influence of Pr.



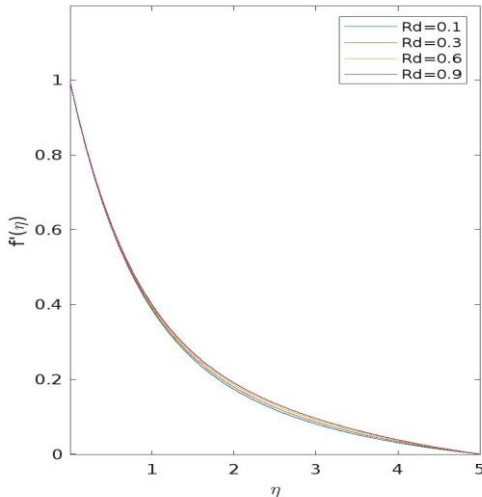
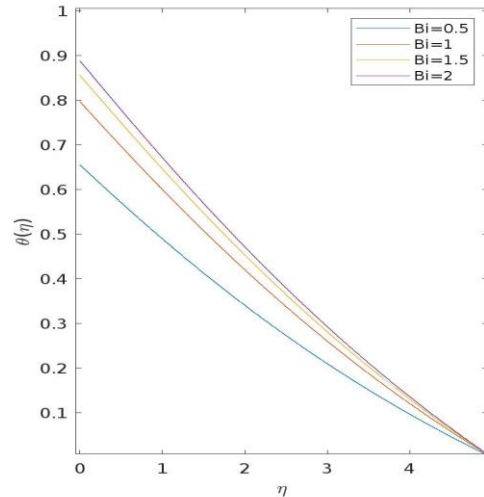
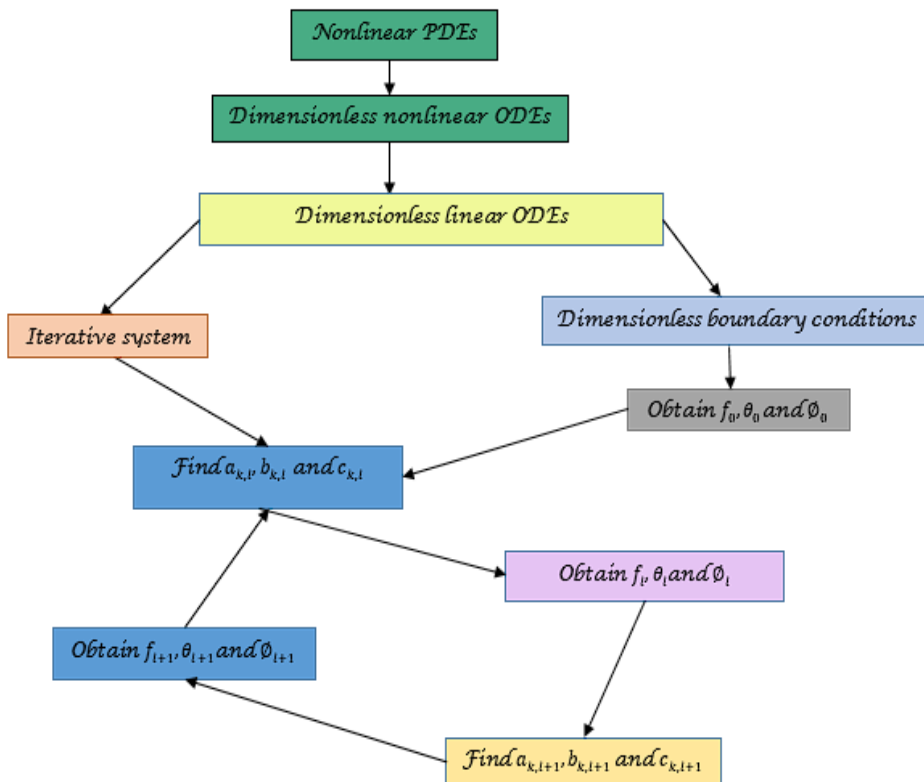
**Fig.8.** Variation of  $f'$  under effect of  $\beta$ .



**Fig.9.** Variation of  $f'$  under influence of Le.



**Fig.10.** Variation of  $\phi$  under effect of Sr.

**Fig. 11.** Influence of  $Rd$  on  $f'$ .**Fig. 12.** Impact of  $Bi$  over  $\theta$ .**Fig. 13.** Quasi-linearized Polynomial Collocation Method algorithm.

## 5. Conclusions

This paper presents an effective numerical technique for solving magnetohydrodynamic Casson nanofluid mixed convection flow using a spectral collocation scheme, along with the quasi-linearization method based on the Taylor series formula. The solution curve is then interpolated using the MATLAB program. We conducted a residual error and convergence analysis, shown in Tables 1-2, at the uniform points concerning the step size. Additionally, variation of the skin friction coefficient, Nusselt number, and Sherwood number is examined

under the influence of the physical parameters shown in Table 3. Lastly, the effects of different values of the physical parameters on the velocity profile, dimensionless temperature, and nanoparticle concentration are analyzed as shown in Figures 1-12.

## References

- [1] H. Alfvén, “Existence of electromagnetic-hydrodynamic waves,” *Nature*, vol. 150, pp. 405–406, Oct. 1942, DOI:10.1038/150405d0.
- [2] J. Buongiorno, “Convective Transport in Nanofluids,” *J. Heat Transfer*, vol. 128, no. 3, pp. 240–250, Mar. 2006, DOI:10.1115/1.2150834.
- [3] O. T. Bafakeeh et al., “Hall current, and Soret effects on unsteady MHD rotating flow of second-grade fluid through porous media under the influences of thermal radiation and chemical reactions,” *Catalysts*, vol. 10, p. 1233, 2022.
- [4] R. Chintalapudi, H. Koti, B. S. Reddy, & K. Saritha, “Mechanisms of diffusion thermo and thermal diffusion on MHD mixed convection flow of Casson fluid over a vertical cone with porous material in the presence of thermophoresis and a Brownian motion,” *J. Adv. Res. Numer. Heat Transfer*, vol. 17, pp. 29–43, 2024.
- [5] E. Homan & K. H. Faraidun, “Nonpolynomial spline interpolation for solving fractional subdiffusion equations,” *Math. Probl. Eng.*, vol. 2022, Art. 7354121.
- [6] N. Gulle & R. Kodi, “Soret radiation and chemical reaction effect on MHD Jeffrey fluid flow past an inclined vertical plate embedded in porous medium,” *Materials Today: Science Direct*, vol. 50, pp. 2218–2226, 2022.
- [7] R. Kodi, R. Vaddeman, & O. Mopuri, “Effects of radiation absorption and aligned magnetic field on MHD Casson fluid past an inclined vertical porous plate in porous media,” in *Simulation and Analysis of Mathematical Methods in Real-Time Engineering Applications*, vol. 4, pp. 273–291, 2021.
- [8] R. Kodi et al., “Unsteady magneto-hydro-dynamics flow of Jeffrey fluid through porous media with thermal radiation, Hall current, and Soret effects,” *J. Magn. Magn. Mater.*, vol. 582, Art. 171033, 2023.
- [9] S. Li et al., “Effects of activation energy and chemical reaction on unsteady MHD dissipative Darcy–Forchheimer squeezed flow of Casson fluid over horizontal channel,” *Sci. Rep.*, vol. 13, Art. 2666, 2023.
- [10] A. S. M. Muhammad, K. H. Faraidun, & F. I. Hajar, “Numerical study of stagnation point flow of Casson–Carreau fluid over a continuous moving sheet,” *AIMS Math.*, vol. 3, pp. 7005–7020, 2023.
- [11] M. A. S. Murad & K. H. Faraidun, “Computational technique for the modeling on MHD boundary layer flow unsteady stretching sheet by B-spline function,” in *2022 Int. Conf. Comput. Sci. Softw. Eng. (CSASE)*, 2022, Art. 9786654.
- [12] D. Pal, G. Mandal, & K. Vajravelu, “Flow and heat transfer of nanofluids at a stagnation point flow over a stretching/shrinking surface in a porous medium with thermal radiation,” *Appl. Math. Comput.*, vol. 238, pp. 208–224, 2014.
- [13] K. V. Raju, R. Mohanaramana, R. S. Sudhakar Reddy, & K. Raghunath, “Chemical radiation and Soret effects on unsteady MHD convective flow of Jeffrey nanofluid past an inclined semi-infinite vertical permeable moving plate,” *Commun. Math. Appl.*, vol. 1, pp. 237–255, 2023.
- [14] R. Vaddeman, S. Ganta, & R. Kodi, “Effects of Hall current, activation energy, and diffusion thermo of MHD Darcy-Forchheimer Casson nanofluid flow in the presence of Brownian motion and thermophoresis,” *J. Adv. Res. Fluid Mech. Therm. Sci.*, vol. 105, pp. 129–145, 2023.
- [15] R. Vaddeman, R. Kodi, & O. Mopuri, “Characteristics of MHD Casson fluid past an inclined vertical porous plate,” *Mater. Today: Proc.*, vol. 49, pp. 2136–2142, 2022.

- [16] M. Sari , S. A. Tahir, "Synchronization of the nonlinear advection-diffusion-reaction processes," *Sigma J. Eng. Nat. Sci.*, vol. 44, pp. 11970, 2020.
- [17] M. A. S. Seddeek, "Effects of radiation and variable viscosity on an MHD free convection flow past a semi-infinite flat plate with an aligned magnetic field in the case of unsteady flow," *Int. J. Heat Mass Transfer*, vol. 45, pp. 931–935, 2002.
- [18] M. Turkyilmazoglu, "Exponential nonuniform wall heating of a square cavity and natural convection," *Chin. J. Phys.*, vol. 77, pp. 2122–2135, 2022.
- [19] R. Viskanta , R. J. Grosh, "Boundary layer in thermal radiation absorbing and emitting media," *Int. J. Heat Mass Transfer*, vol. 5, pp. 795–806, 1962.
- [20] A. M. Abed et al., "Inspection of numerical and fractional CMC and water-based hybrid nanofluid with power law and non-singular kernel: a fractal approach," *Int. J. Thermofluids*, vol. 23, Art. 100772, 2024.
- [21] M. W. AbdulRidha, H. A. Kashkool , A. H. Ali, "Petrov-discontinuous Galerkin finite element method for solving diffusion-convection problems," *Ital. J. Pure Appl. Math.*, vol. 2322, 2022, DOI:10.1088/1742-6596/2322/1/012007.

## Nomenclature

| Symbol                  | Description   |
|-------------------------|---|
| MHD                     | Magnetohydrodynamics  |
| $u$                     | Velocity component in $x$ –direction  |
| $v$                     | Velocity component in $y$ –direction  |
| $\rho$                  | Density   |
| $T$                     | Temperature   |
| $\nu$                   | Kinematic viscosity   |
| $f'(\eta)$              | Dimensionless velocity profile  |
| $\theta(\eta)$          | Non dimensional temperature   |
| $\phi(\eta)$            | Nanoparticle concentration  |
| $\frac{1}{Re_x^2 Cf}$   | Skin friction coefficient   |
| $\frac{1}{Re_x^2 Nu_x}$ | Nusselt number  |
| $\frac{1}{Re_x^2 Sh_x}$ | Sherwood number   |
| $\beta$                 | Casson parameter  |
| $M$                     | Magnetic parameter, $M = \frac{\sigma B_0^2 x}{\rho R a_x^2}$                 |
| $R_d$                   | Radiation parameter, $R_d = \frac{14\sigma^* T_{\infty}^3}{3kK^*}$            |
| $P_r$                   | Prandtl number, $P_r = \frac{\nu_p C_p}{k}$                                   |
| $N_b$                   | Brownian motion parameter, $N_b = \frac{\tau D_B (C_w - C_{\infty})}{\alpha}$ |

|          |   |
|----------|---|
| $N_t$    | Thermophoresis parameter, $N_t = \frac{\tau D_T (T_w - T_\infty)}{\alpha}$  |
| $D_u$    | Dufor parameter, $D_u = \frac{D_M k_T (C_w - C_\infty)}{C_s C_p v a^2 (T_w - T_\infty)}$                              |
| $L_e$    | Lewis number, $L_e = \frac{\alpha}{D_B}$  |
| $S_r$    | Soret number, $S_r = \frac{D_m k_T (T_w - T_\infty)}{T_m \alpha_m (C_w - C_\infty)}$                                  |
| $Bi$     | $B_i = \frac{h_f x}{\frac{1}{k R} a_x^2}$   |
| $Ra_x$   | Rayleigh number, $Ra_x = \frac{g \beta \rho_{f_\infty} (T_w - T_\infty) (1 - C_\infty) \cos(\gamma) x^3}{\mu \alpha}$ |
| $\alpha$ | Thermal diffusivity, $\alpha = \frac{k}{\rho c_p}$  |
| w        | Quantities at wall  |
| $\infty$ | Quantities at free stream   |

---

## طريقة التجميع متعدد الحدود شبه الخطية المتعددة الحدود لحل الحراري المختلط للسوائل كاسون MHD النانوية المختلطة

فريدون قادر حمه صالح<sup>١,\*</sup>, بهلين دلشاد ياسين<sup>٢</sup>, شكو علي طاهر<sup>٣</sup>

<sup>١</sup>جامعة السليمانية التقنية، معهد بكرجو التقني، السليمانية، العراق.

<sup>٢</sup>جامعة السليمانية، قسم الرياضيات، كلية التربية، السليمانية، العراق.

<sup>٣</sup>جامعة السليمانية، قسم الرياضيات، كلية العلوم، السليمانية، العراق.

### معلومات البحث

### الملخص

ركزت الدراسة الحالية على التحليل العددي والبياني لأآلية الانتشار الحراري والانتشار الحراري فوق سريان مائع كاسون مختلط الحمل الحراري فوق مخروط عمودي مع مادة مسامية تحت تأثيرات الحركة البراونية والرحلان الحراري. وباستخدام المتغيرات القابلة للتحويل، يتم تحويل النموذج المقترن إلى نظام من متغيرات متغيرة غير خطية ODEs. ثم يتم إنشاء الحلول التقريبية باستخدام نماذج متعددة الحدود بالاقتران مع التجميع الطيفي. يتم فحص تأثير بعض المعلومات المهمة، مثل معلمـة الحركة البراونية، ورقم براندل، والمعلمـة المغناطيسية، ومعلمـة كاسـون، ومعلمـة لوـيس، ومعلمـة دوفور، ومعلمـة سورـيت، ومعـامل السـرعة، ودرجـة الحرـارة، والانتـشار، ومعـامل احتـكـاك الجـلد، ورقم نوسـيلـيت، ورقم شـيرـوـود، عـدـيـا. كما يتم حلـ العـدـيد من الحالـات ومقارـنتـها بـبيانـا، مما يـوضـح الدـقة المـحسـنة للنهـج الحالـي.

|          |                |
|----------|----------------|
| الاستلام | 28 اذار 2025   |
| المراجعة | 2 حزيران 2025  |
| القبول   | 12 حزيران 2025 |
| النشر    | 30 حزيران 2025 |

### الكلمات المفتاحية

ديناميكا المواقع، الاندراج متعدد الحدود، المواقع النانوية، التجميع الطيفي.

**Citation:** F. K. Hamasalh et al., J.Basrah Res. (Sci.) 51(1),182 (2025).  
**DOI:** <https://doi.org/10.56714/bjrs.51.1.16>

\*Corresponding author email: faraidun.hamasalh@spu.edu.iq



©2022 College of Education for Pure Science, University of Basrah. This is an Open Access Article Under the CC by License the [CC BY 4.0](#) license.

ISSN: 1817-2695 (Print); 2411-524X (Online)  
Online at: <https://jou.jobrs.edu.iq>